SANDIA REPORT
SAND2003-8137
Unlimited Release
Printed March 2003

# Computer Simulation of Boundary Effects on Bubble Growth in Metals Due to He

J.A. Zimmerman

Prepared by
Sandia National Laboratories
Albuquerque, New Mexico 87185 and Livermore, California 94550

Sandia is a multiprogram laboratory operated by Sandia Corporation,
a Lockheed Martin Company, for the United States Department of Energy's
National Nuclear Security Administration under Contract DE-AC04-94AL85000.



Sandia National Laboratories

Issued by Sandia National Laboratories, operated for the United States Department of Energy by Sandia Corporation.



Available to DOE and DOE contractors from
U.S. Department of Energy
Office of Scientific and Technical Information
P.O. Box 62
Oak Ridge, TN 37831

Telephone: (865)576-8401
Facsimile: (865)576-5728
E-Mail: reports@adonis.osti.gov
Online ordering: http://www.doe.gov/bridge

Available to the public from
U.S. Department of Commerce
National Technical Information Service
5285 Port Royal Rd
Springfield, VA 22161

Telephone: (800)553-6847
Facsimile: (703)605-6900
E-Mail: orders@ntis.fedworld.gov
Online order: http://www.ntis.gov/help/ordermethods.asp?loc=7-4-0#online

SAND2003-8137
Unlimited Release
Printed March 2003

# Computer Simulation of Boundary Effects on Bubble Growth in Metals Due to He

J.A. Zimmerman
Science-based Materials Modeling Department

Sandia National Laboratories
P.O. Box 969
Livermore, CA 94551

## Abstract

Atomistic simulation methods were used to investigate and identify the relevant physical mechanisms necessary to describe the growth of helium gas bubbles within a metal lattice. Specifically, molecular dynamics simulations were performed to examine the material defects that originate from growing spherical He bubbles in a palladium crystal. These simulations consist of a model system containing bubbles within a metal and near a free surface. The simulation code employed was ParaDyn using the Embedded Atom Method to model the constitutive properties of Pd atoms in a FCC lattice. The results of these simulations are compared with previously run calculations of He bubbles in a bulk lattice [1]. These simulations show the influence of the free surface on defect creation and evolution. Features compared include the formation of inter-bubble dislocations, bubble pressure and swelling as functions of He to metal (He/M) concentration.

**Keywords:** atomistic simulation; crystal; free surface; helium; bubbles; palladium; dislocations; boundary effects.

This page intentionally left blank.

# Contents

**Introduction** 7

**Computational Methods** 9
- Simulation Methodology . . . 9
  - Equations of Motion . . . 9
  - Ensembles and Boundary Conditions . . . 9
  - Material Model . . . 10
  - Bubble Growth Model . . . 11
- System Geometry . . . 11

**Simulation Results** 13
- System Statisitcs . . . 13
- Material Defects . . . 15

**Discussion of Simulation Results** 19

**Summary and Future Directions for Research** 25

**Bibliography** 27

**Acronyms and Symbols** 29

**Distribution** 31

# List of Figures


1 System Geometry. . . . . 12
2 Bubble pressure as a function of He content. . . . . 13
3 System pressure and temperature as a function of He content. . . . . 14
4 Volume fraction of He and swelling as a function of He content. . . . . 15
5 Dislocations and defects in the free surface and bulk simulations. . . . . 16
6 Top view of the free surface simulations. . . . . 17
7 3-D views of the free surface simulations. . . . . 18
8 Normal stresses for the system as a function of He content. . . . . 20
9 2-D thick-walled cylinder with a pressurized hole. . . . . 21
10 FE mesh of a pressurized cylindrical hole. . . . . 22
11 FE mesh of a region with multiple pressurized holes. . . . . 23

# Introduction

Helium (He) is a by-product of the decay of tritium. The insolubility of He with metals allows He atoms to be retained within the material by clustering at defects like dislocations. This clustering leads to the formation of nano-scale bubbles, which grow as the concentration of He within the metal increases. The development of these bubbles has been observed experimentally within palladium [2, 3] and vanadium [4] tritide alloys, and is almost certainly linked to additional dislocations and other defects, *e.g.* clusters of self-interstitial atoms (CSIA), that form during periods of bubble growth. Of particular importance is the observation that once a critical concentration of helium to metal atoms (He/M) is reached, helium gas is released from the material at an accelerated rate. For example, examination of aged palladium tritide PdT samples has revealed that when the ratio He/M reaches values between 0.5 to 0.55 [5, 6], a large amount of $^3$He is released. This critical ratio has been observed to vary as low as 0.3, depending upon system temperature, and whether or not tritium replenishment occurs.

In an effort to understand the material defects created during He bubble growth and the mechanical interaction between these defects and the bubbles themselves, as well as predict the physical mechanism responsible for accelerated release of $^3$He gas, analytical [7, 8, 9, 10] and computational [1, 11] models have been developed to study these processes. Originally, the favored theory involved the punching of prismatic dislocation loops [8, 9, 10, 11] as the mechanism by which He bubbles could expand. These models produced reasonable predictions for bubble pressure and lattice swelling as a function of He content. Later models hypothesized the formation of dislocation pipes or threads [7], which could also act as diffusion paths for He atoms to traverse between bubbles and, eventually, to a grain boundary or a free surface culminating in a release of He gas. Support for this analytical model was shown through molecular dynamics calculations performed by Foiles and Hoyt [1]. Their simulations displayed the formation of dislocation threads that interconnected the bubbles, as well as other material defects such as vacancies and stacking fault tetrahedra. However, because their simulation utilized full periodic boundary conditions in order to represent a region of bulk crystal, it was not clear that these threads would serve as a path for accelerated release, or even what interaction they would have with a free surface or other geometrical inhomogeneity.

The goal of this research is to investigate and identify the relevant physical mechanisms necessary to describe the growth of He gas bubbles in metals. Specifically, criteria are needed for predicting the accelerated release of He from implanted and aged materials. Molecular dynamics simulations were used to examine the material defects that originate from growing spherical He bubbles within a Pd lattice. These simulations consist of a model system containing bubbles within a bulk metal and near a free surface. The simulation code employed was ParaDyn using the Embedded Atom Method to model the constitutive properties of atoms in Pd. The results of these simulations are compared with previously run calculations of He bubbles in a bulk lattice. This simulation set shows the influence of the free surface on defect creation and evolution. Features compared include the formation

of inter-bubble dislocations, bubble pressure and swelling as functions of He concentration. Examination of pressure, volume and swelling characteristics of the systems and the bubbles for the free surface calculations reveals the need for improving the implementation of non-periodic boundary conditions.

# Computational Methods

Use of particle simulation methods is widespread in today's age of computational materials analysis. There are many research problems in the study of both fluids and solids which require examination of the behavior of individual particles, in place of the continuum mechanical approach of treating a material as a continuous and homogeneous medium. Such work includes study of the mechanics of fracture at a crack tip [12, 13] as well as the effect of defects such as dislocations, vacancies, interstitials, voids and inclusions on mechanical behavior.

## Simulation Methodology

### Equations of Motion

Molecular dynamics (MD) is perhaps the most straightforward type of simulation method used by researchers to analyze materials problems. It involves deriving the equations of motion for a system comprised of a large number of particles, which results in a set of coupled ordinary differential equations, and solving these equations by discretization of time and approximation of time derivatives. The governing equation of motion is Newton's $2^{nd}$ law,

$$F_i^\alpha = m_\alpha \ddot{r}_i^\alpha. \tag{1}$$

In this expression, $F_i^\alpha$ denotes the force in the $i^{th}$ direction acting on particle $\alpha$, $m_\alpha$ denotes that particle's mass, and $r_i^\alpha$ denotes the $i^{th}$ component of the particle's position. The notation $\ddot{z}$ is equivalent to the second time derivative, $\frac{d^2z}{dt^2}$, of the variable $z$. As a convention, lower case Roman letters ($i$, $j$, $k$) denote a Cartesian coordinate direction ($i = 1, 2, 3$) and lower case Greek letters ($\alpha$, $\beta$) denote the number designation for a particle belonging to a system of $N$ particles.

### Ensembles and Boundary Conditions

Although the equations of motion and the numerical techniques used to solve those equations are of the utmost importance in examining the behavior of a system of particles, also of significance are the constraints applied to the system. This involves a discussion of two additional topics, ensemble type and boundary conditions. This section will address these issues as they relate to a MD simulation.

The explanation of atomistic simulation necessitates a discussion about statistical mechanics. Statistical mechanics is the method by which individual properties of particles from a system are used to calculate macroscopically observable and measurable quantities. A well known example is temperature, which is merely a measurement of the average kinetic energy of all particles that make up a system or body. These systems are referred to as ensembles and the observable quantities as ensemble averages. An atomistic simulation is usually constrained such that certain ensemble averages remain constant. For instance, the equations of motion presented above are valid for an ensemble in which the number of particles, $N$, and

total energy, $E$, are constants. In most MD simulations, a constant volume, $V$, is specified either by employing rigid boundaries which provide external forces on some atoms, or by enforcing periodic boundary conditions, the latter of which will be discussed shortly. Such systems are called *microcanonical* or NVE ensembles, after the three system quantities held constant.

A common alternative is a system in which both temperature, $T$, and pressure, $P$, are held constant instead of system energy and volume. This ensemble is known as the isothermal-isobaric or NPT ensemble. Proper treatment of the NPT ensemble is done by allowing the system of particles to change volume (for constant pressure) and total energy (for constant temperature) by the addition of extra degrees of freedom to the equations of motion. The technique for adding extra variables necessary for such simulations can be found in the book by Allen and Tildesley [14]. In these simulations, the desired temperature is 500 K and the desired pressure is zero. The extra degrees of freedom were used to alter the system boundaries in order to maintain this zero pressure condition, resulting in a swelling of the system that can be quantified.

The simulations performed for this work used periodic boundary conditions in order for the atomic system to represent a slab of material of much larger extent in certain dimensions. If an atom is moved beyond the system's boundaries, then its position is recalculated with the appropriate length subtracted, effectively moving the atom to other side of the simulation region. In this way, it can be considered that the atom has left the simulation region while its periodic image has entered it. Atoms near the periodic boundaries in these systems have the same energies and forces as bulk atoms because they effectively "feel" the periodic images of other atoms as their nearest neighbors. Thus, periodic boundary conditions allow a small simulation region with a limited number of particles to successfully model bulk material, enabling calculation of bulk properties. These simulations also contain free surfaces. In the directions of these surfaces, the atomic motion is not constrained and periodic images are not used.

### Material Model

Inter-atomic forces are derivable from the potential energy of the system, $E$. $E$ is calculated using the Embedded Atom Method (EAM), developed by Foiles, Baskes and Daw [15, 16],

$$E = \frac{1}{2}\sum_{\alpha=1}^{N}\sum_{\beta\neq\alpha}^{N}\phi_{\alpha\beta}(r^{\alpha\beta}) + \sum_{\alpha=1}^{N}F_{\alpha}(\rho_{\alpha}), \tag{2}$$

where there are $N$ atoms within the system. In this expression, each atom's potential energy is derived from two separate contributions. The first is the summation of pair potential energy between a given atom $\alpha$ and its neighbors $\beta$, $\phi_{\alpha\beta}$. These pair potential energies depend only on the radial separation of the two atoms, $r^{\alpha\beta}$ , and are representative of the repulsion between the ionic cores of atoms. The second contribution, $F_{\alpha}$, is the energy necessary to "embed" atom $\alpha$ in an electron gas of some density $\rho_{\alpha}$ composed of contributions from all

the neighbors $\beta$ of the atom. The electron density is assumed to be a linear superposition of spherically-averaged atomic charge densities,

$$\rho_\alpha = \sum_{\beta \neq \alpha}^{N} f_\beta \left( r^{\alpha\beta} \right), \tag{3}$$

where $f_\beta$ is an atomic charge density function.

The force on each atom can be determined by taking the derivative of $E$ with respect to its position vector. Thus,

$$\mathbf{F}^\alpha = -\sum_{\beta \neq \alpha}^{N} \left[ \left( F'_\alpha(\rho_\alpha)\, f'_\beta\left(r^{\alpha\beta}\right) + F'_\beta(\rho_\beta)\, f'_\alpha\left(r^{\alpha\beta}\right) \right) + \phi'_{\alpha\beta}\left(r^{\alpha\beta}\right) \right] \frac{\mathbf{r}^{\alpha\beta}}{r^{\alpha\beta}} \tag{4}$$

The EAM potential parameters used for this research were the same ones used in the work by Foiles and Hoyt [1], and are detailed in Appendix A of that reference.

### Bubble Growth Model

Growth of He bubbles is simulated by using several external repulsive potentials with ever-increasing ranges of interaction. Each potential is centered at a specific position $\mathbf{R}^B$ (B = 1, 2, 3 or 4) with respect to the crystal lattice. The volume of these bubbles is increased linearly with time, resulting in bubbles of radius $R$ for which $R \sim t^{1/3}$. The repulsive potential functions are functions of the variable $r^{\alpha B} \equiv \|\mathbf{r}^\alpha - \mathbf{R}^B\|$ for cases where $r^{\alpha B} < R$. Here, $\mathbf{r}^\alpha$ is the position of atom $\alpha$, $\mathbf{R}^B$ is the position of bubble B and $R$ is the radius of bubble B. Foiles and Hoyt [1] have already used this method to simulate bubble growth within a bulk metal lattice. Details about the functional form and parameters of the potentials can be found in Appendix B of [1].

Molecular dynamics simulations using EAM are executed using the ParaDyn code, developed by Stephen Foiles and Steve Plimpton. This code is written in FORTRAN 77 and uses Message Passing Interface (MPI) commands for parallel processing operations [17]. The simulation of bubble growth was broken into 60 separate simulations, each consisting of 50,000 time-steps of 0.005 psec per time-step. Each set used either 64 or 128 nodes, and resulted in a computation time of either 16 or 12 hours, respectively, per simulation. These simulations were performed on the Delmar system, a 256-node cluster located at SNL/CA. Visualization of the simulation data was performed using Xmgr, a data-plotting tool on the local SUN workstation, and EnSight, a finite element visualization tool. Files were stored on the local file-system for CPlant/CA and on the Sandia Mass Storage System.

## System Geometry

The system modeled by this project was a face-centered-cubic (FCC) metal lattice with dimensions of 155.6 Å (x-direction) x 155.6 Å (y-direction) x 210.06 Å (z-direction), consisting of a total of 345,600 atoms. The boundary conditions applied to the system are periodic in

the x-y plane, a free surface at the top, and a fixed surface at the bottom. The fixed surface restricts atoms in the lowest (in the z-direction) plane of atoms to have motion only within the x-y plane. Four bubbles were placed within the lattice in a tetrahedral-like arrangement shown in Figure 1. The positions of the bubbles are held fixed **relative** to the simulation

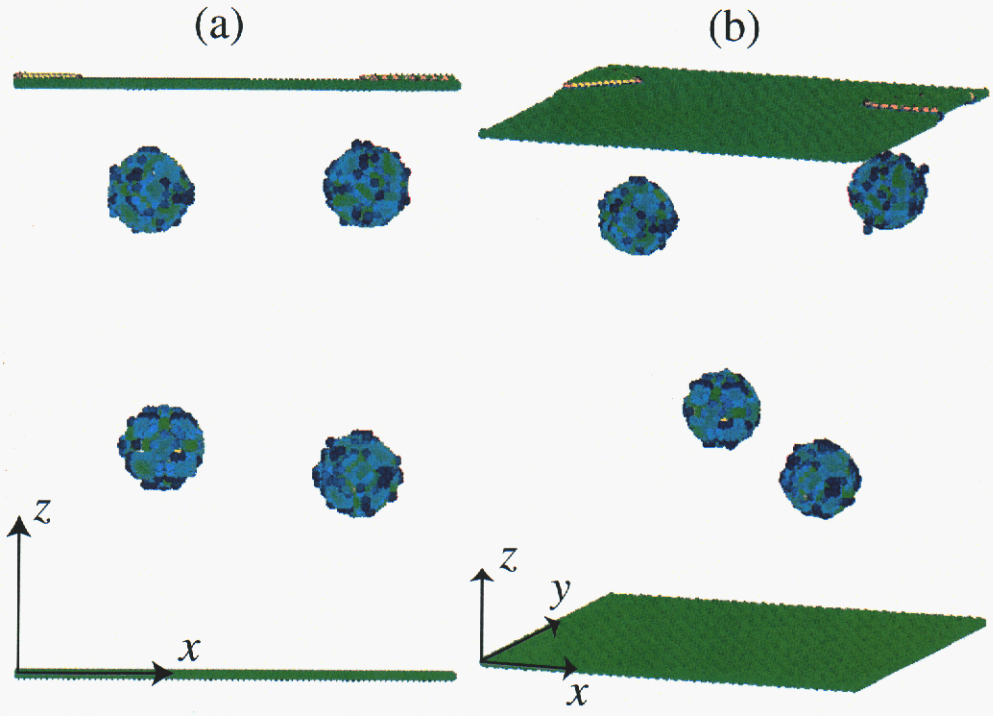


Figure 1: (a) Side and (b) off-diagonal views of the system geometry: a FCC metal lattice containing four growing He bubbles. For clarity, only the bubbles and the top and bottom surfaces are shown.

region. That is, the bubble centers only move within the horizontal (x-y) plane when the system's lengths in those directions are scaled in order to maintain the zero pressure condition. The bubble centers are fixed in the z-direction, since that dimensional length is not scaled due to the rigid (bottom) and free (top) surface boundary conditions.

# Simulation Results

## System Statisitcs

The simulations of bubble growth were executed starting from an initial He concentration of zero up to approximately 36%. Pressure within each bubble is determined from a summation of the magnitudes of forces exerted on the atoms bordering the bubble's surface divided by the bubble's surface area. This pressure is viewed as representative of the effect of containing He gas within the bubble's volume. The plots in Figure 2 show the average bubble pressure as a function of the He content of the system, either as a ratio of He to Pd atoms, or as volume of He present in the system. For comparison, simulation results for a bulk system, *i.e.*

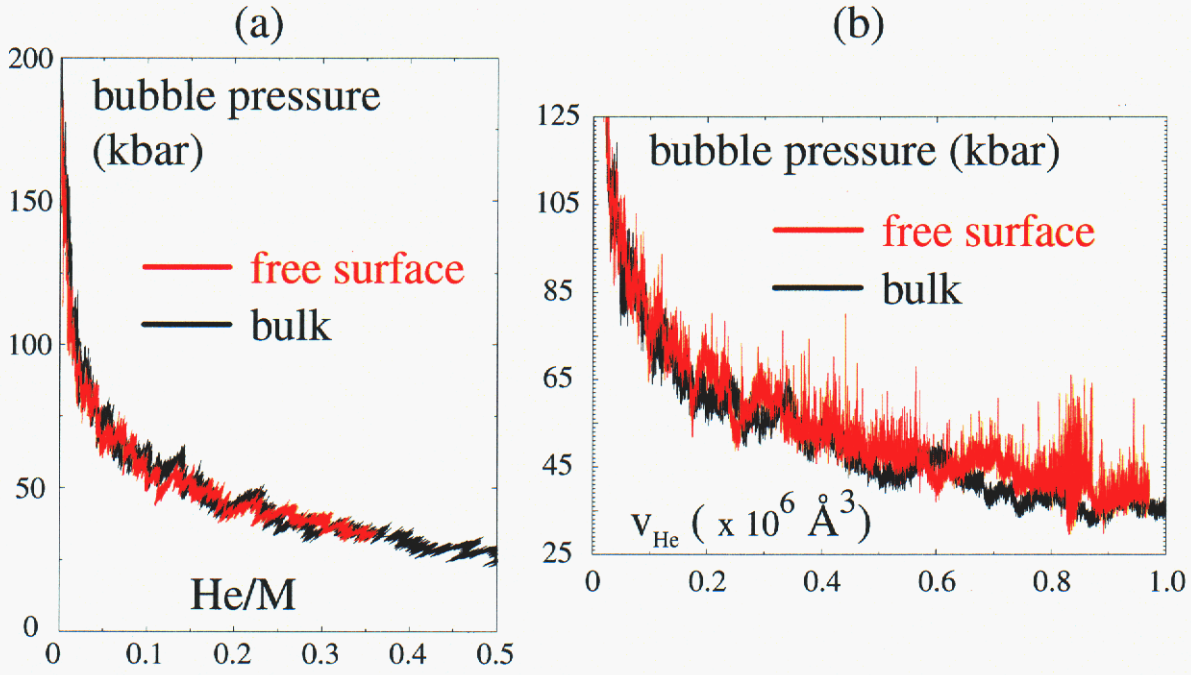


Figure 2: Average bubble pressure as a function of (a) ratio of He to metal atoms, and (b) volume of He.

periodic boundary conditions on all sides, are shown in black while the simulation results for the free surface system are displayed in red. This convention is used for most figures that will follow, unless otherwise noted. Both curves show bubble pressure initially high, but decreasing monotonically with increasing He concentration. In Figure 2(a), the curves are overlapping, an expected result since the same equation of state (the relation between pressure, volume, temperature and density) is used. Examination of Figure 2(b) reveals that the free surface simulation set has slightly higher pressure at a given instant of time, or for a given volume of He in the lattice. This result counters the expectation that a free

surface system would have higher compliance than the bulk system, leading to a lower bubble pressure.

The pressure and temperature of the entire system can be examined in order to assess whether the environmental conditions are the same for the bulk and free surface simulations. This is shown in Figure 3. The system temperature was set to 500 K, a value considerably

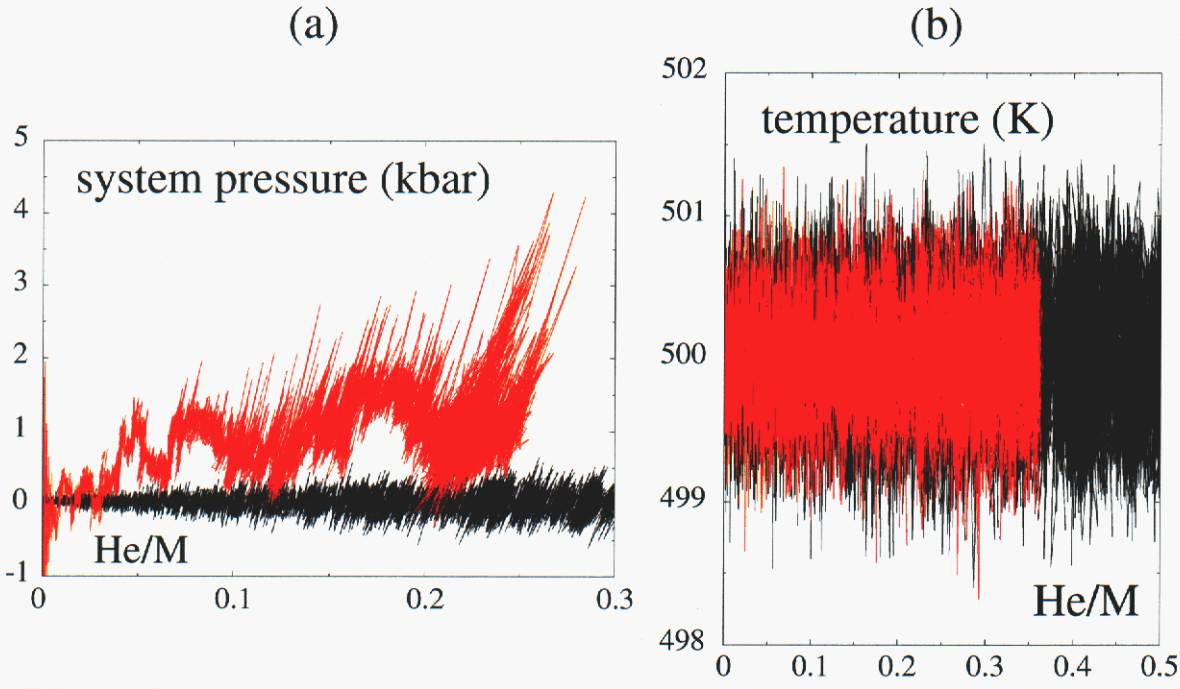


Figure 3: System pressure and temperature as a function of ratio of He to metal atoms.

higher than room temperature, approximately 300 K. This was done purposefully in order to compensate for the short time scale inherent to molecular dynamics simulations. It was assumed that, at higher temperature, metal atoms are more agitated and material defects form sooner than at lower temperature. Also, simulation at 500 K enables these results to be directly comparable with the earlier simulations done in reference [1]. Simulation at lower temperature would presumably produce similar material defects in the metal with only slight shifts of the curves presented here. It is observed that the system temperature is being regulated to 500 K for both simulation sets, within an error of 1.5 degrees Kelvin. System pressure is not as well controlled. Although the system pressure oscillates for the bulk simulations, the mean appears to be zero. However, the oscillations for the free surface system are more extreme in magnitude, and the mean drifts upwards to non-zero values.

Also examined are the volume fraction of He within the Pd lattice and the swelling of the metal. These results are shown in the Figure 4. Figure 4(a) shows that for a given concentration of He, there is roughly the same, or slightly less volume fraction of He for the

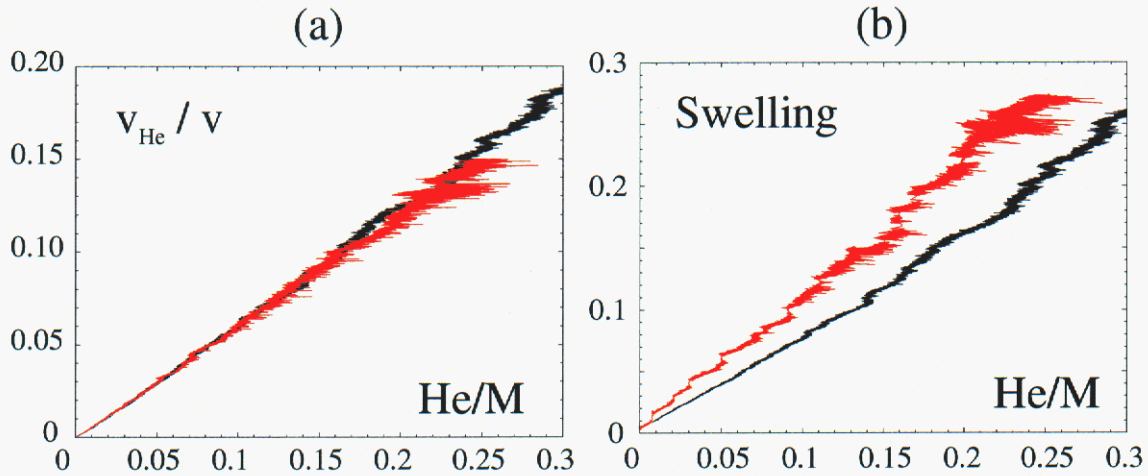


Figure 4: (a) Volume fraction of He and (b) swelling as a function of ratio of He to metal atoms.

free surface simulations as compared with the bulk simulations. This lower volume fraction is an expected result, although a larger difference was anticipated since the initial volume of the lattice itself is 35% higher for the free surface case. Figure 4(b) shows a significantly higher amount of swelling (defined as the change in system volume divided by the initial volume) for the free surface simulations.

## Material Defects

The objective of this project is to investigate the nucleation of dislocations and other material defects that occurs during bubble growth. In order to image the dislocation and stacking fault structures created during bubble growth, the simulation data is filtered using the centro-symmetry parameter developed by Kelchner, Plimpton and Hamilton [18]. This parameter equals a value of zero for atoms that possess a symmetric distribution of near neighbors, such as for a homogeneously deformed bulk lattice, and non-zero values for atoms that border surfaces, dislocation cores and stacking faults. The defects for some of the simulations can be seen in Figure 5. Also shown are the defects for the bulk simulations that correspond to the same bubble volume. In this figure, atoms are colored by their value of the centro-symmetry parameter normalized by the square of the materials lattice constant: dark red is used for the lowest values (above zero) while bright yellow is used for the highest values. Note that the same bubble volume implies a lower He concentration for the free surface simulations, in agreement with the slightly higher pressure mentioned above. Both sets of simulations show dislocation threads connecting bubbles to each other, as well other defects such as vacancies (denoted by the small clusters of visible atoms) and stacking fault tetrahedra (the triangular-faceted structures visible in the free surface simulations at He/M = 0.04 and 0.2,

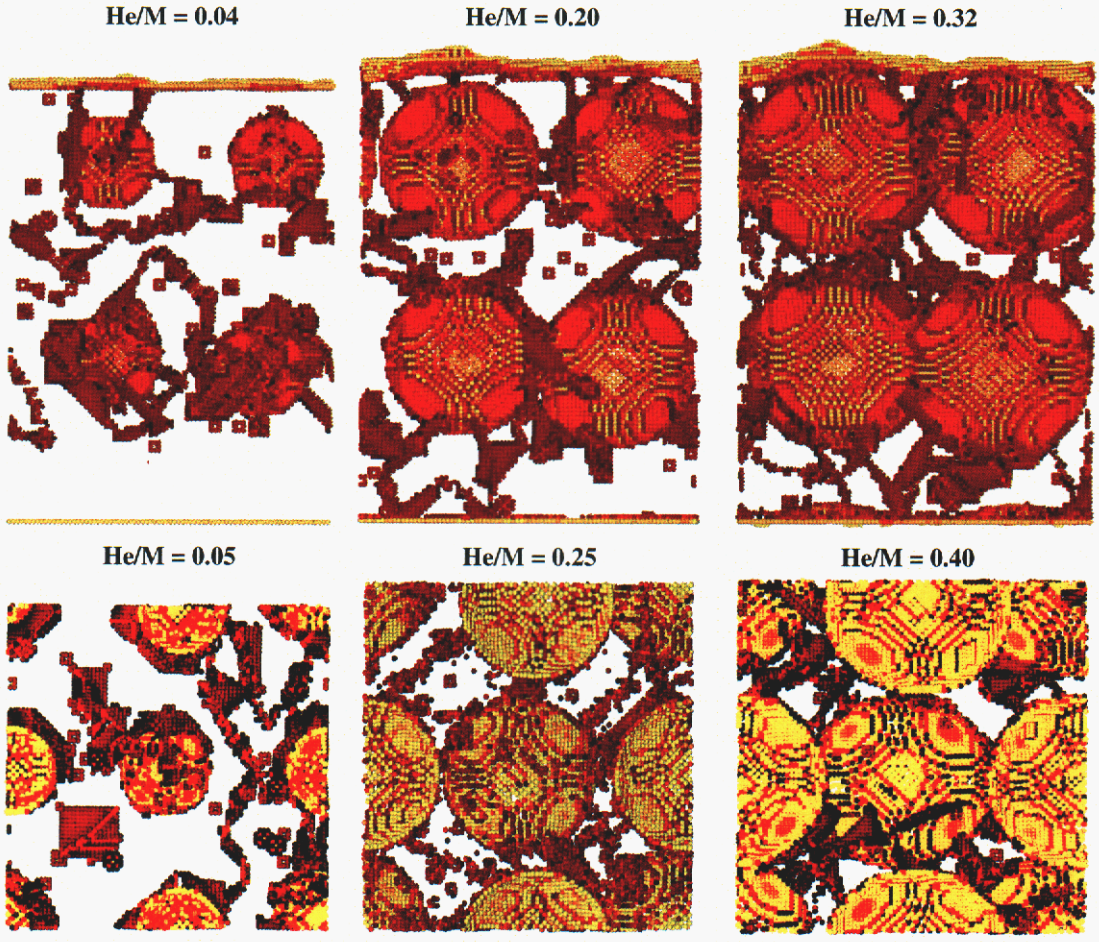


Figure 5: Dislocations, defects and surfaces visible in the free surface (top row) and bulk (bottom row) simulations by using the centro-symmetry parameter.

and in the bulk simulations at He/M = 0.05). In the free surface simulations, the dislocation threads also connect the top-most bubbles with the free surface itself. At the early stages of dislocation nucleation (He/M = 0.04) in the free surface simulations, the dislocation threads appear to connect multiple points on a single bubbles surface, but remain attached only to that single bubble, except for the bubble at the upper-left, which does have threads connected to the free surface. At higher He concentrations (He/M = 0.2 and 0.32), the threads inter-connect the bubbles. Both simulations appear to show an increasing amount of defects with increasing He concentration, although a variable still needs to be developed to quantify the dislocation/defect content within a simulated crystal lattice.

Visible in the figures of the free surface simulation seen above, is the distortion and roughening of the free surface itself. This can be seen more clearly in Figure 6, which shows the atoms that comprise the top surface of the crystal, colored by the height, *i.e.* z-coordinate value. The figure shows a large variation in surface height, with a magnitude of variation of

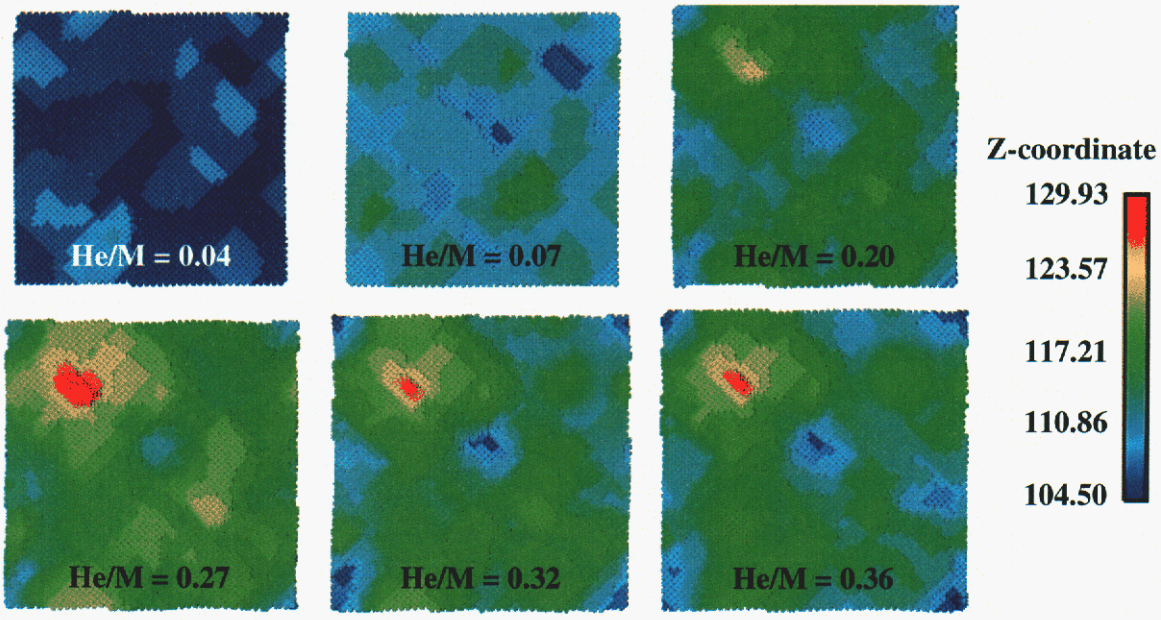


Figure 6: Top view of the free surface simulations. Height is indicated by the color key to the right.

approximately 25.4 Å, a distance spanning 6 unit cells or 12 atomic planes. An interesting feature of the surface roughening is that the portion of the surface at the peak height (located in the upper-left corner of each figure) is at a position with no bubble beneath it. Also, there is no matching peak at the surface position diagonally across from it (lower-right) that also lacks a bubble beneath the surface. This inhomogeneity is a product of dynamical motion, and shows that mechanical stresses are relieved in a specific area, thus negating the need for relief in symmetrically equivalent positions. The surface roughness figure does still possess

some natural symmetry, such as the lowest surface located in the center of the surface area, and at equivalent position at the corner of the side periodic boundaries.

Also of interest is the fact that the highest value of surface height is not attained at the highest He/M ratio, but at an earlier ratio of 27%. Further examination of the dislocation and defect structure at that concentration shows a large amount of defects present at this concentration. This is shown in Figure 7. Compared with the earlier He/M ratio of 0.14 and

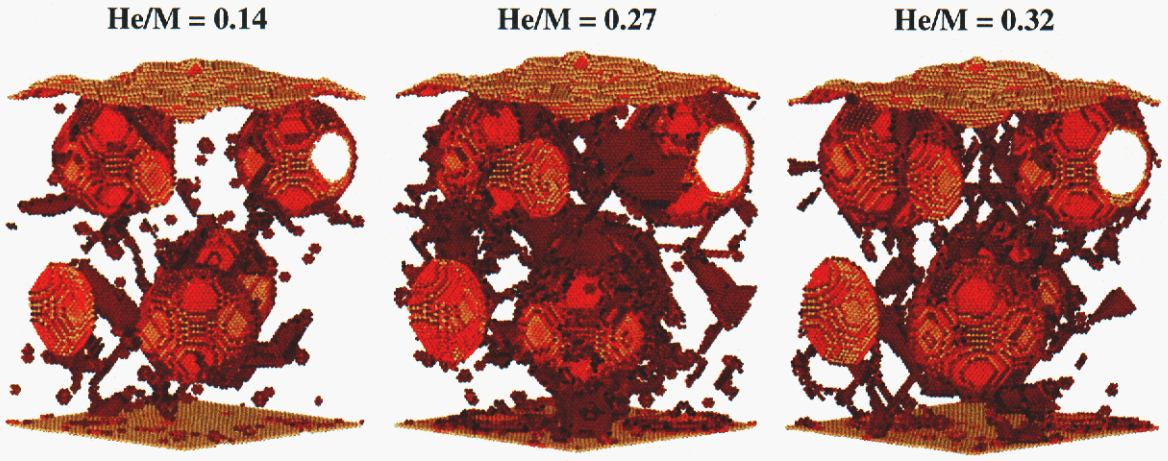


Figure 7: 3-dimensional views of the free surface simulations. Atoms are made visible and colored by the centro-symmetry parameter.

the later ratio of 0.32, considerably more defects are present at He/M = 0.27. These defects are not only in the form of threading dislocations and voids, but a large amount of stacking fault planes are adjacently connected to several of the bubbles. The stacking faults could also be planes of punched dislocation loops, however they appear triangular in shape, which might not be consistent for spherical bubbles. How the FCC crystal structure affects the shape of punched dislocation loops is unknown, and there has been little research involving experimental observations of punched loops for multiple bubble systems. The abundance of defected crystal for this specific He/M ratio may indicate the absence of mechanisms in the model, which would otherwise lead to the accelerated release of He gas from the bubbles. Further research will be conducted to investigate this hypothesis.

## Discussion of Simulation Results

These simulations provide much insight into the mechanics governing the nucleation of dislocations and other material defects during He bubble growth in a metal lattice. The ability to predict these processes is critical for evaluating the stability of aged and implanted material containing inert gases. This research, like the work in [1], clearly shows that the preconception of bubble growth solely by dislocation loop punching is erroneous. Loop punching (LP) theory predicts prismatic dislocation loops that originate from the surface of bubbles and then separate from the bubbles themselves. The simulations performed show a dominance of threading dislocations, which continue to remain attached to the He bubbles, and the presence of additional material defects not accounted for in earlier theories, such as vacancies, voids, and stacking fault tetrahedra. LP theory also predicts the interaction of punched loops causing an eventual increase in bubble pressure with increasing He concentration. These simulations show that for both cases, bubble pressure monotonically decreases with increasing He/M ratio. Increases in bubble volume simply lead to increased production of dislocation threads and stacking fault defects.

The material defects observed for the free surface simulations differ from those in the bulk simulations in that a number of dislocation threads connect the higher bubbles to the free surface. Also, the dislocation distribution appears uniformly random for the bulk simulations. In contrast, more dislocations are present between the four bubbles and between the higher bubbles and the free surface than between the lower bubbles and the bottom, fixed surface. However, at higher He/M ratios, some dislocations are present in this lower region, and connect the bubbles to the bottom surface layer. This indicates that a more realistic boundary condition may be required to truly emulate a system of much greater thickness for the He/M ratios at which accelerated release of He gas would occur.

There is some concern in the interpretation of results of the free surface simulations, as compared with the bulk simulation. One issue is the variation of system pressure with increased He/M ratio. Unlike the bulk simulations, which oscillate about a zero system pressure, the pressure for the free surface system increases with age, although large oscillations are present for both simulation sets as shown in Figure 3. The cause of this excess compression in the system can be attributed to the component of stress for the direction normal to the free surface, the z-direction for the simulation region. Figure 8 shows the normal stresses for this direction, as well as the x- and y-directions which are parallel to the free surface. It's clear that although large magnitude oscillations are present, the system-averaged stresses $\sigma_{xx}$ and $\sigma_{yy}$ have a mean value of zero with increasing He concentration, while the mean value of $\sigma_{zz}$ tends towards negative (compressive) values.

Several aspects of the free surface simulations were examined in order to determine the cause of this excess compression. The most obvious feature of the simulated system to be scrutinized is the fixed boundary condition for the bottom-most atomic plane. These atoms are allowed to move within the horizontal x-y plane, but are restricted from motion in the vertical z-direction. This is done so that the system represents a semi-infinite solid, with the hope that the interactions between the bubbles and the free surface will be more significant to

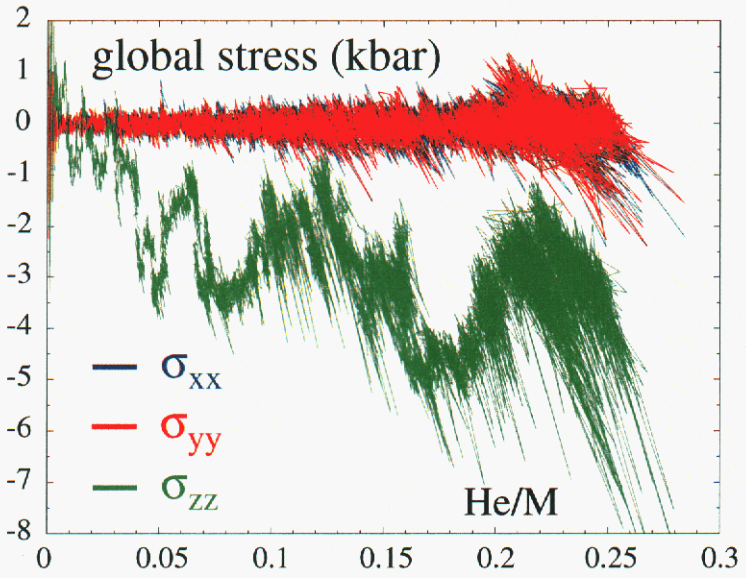


Figure 8: Normal stresses for the system as a function of ratio of He to metal atoms.

the system's behavior than any interactions between the bubbles and this fixed plane. Also, the impact of fixing this atomic layer should be minimal as only 6400 of the 345,600 atoms (1.85%) are subject to this boundary condition. However, the absence of neighbors below these atoms results in a higher atomic potential energy, and may also lead to some amount of surface stress. It is, as yet, unclear what the effect this additional stress contribution should have on the system pressure, and it may also be affecting the average bubble pressure observed during bubble growth.

The focus on the fixed boundary condition, rather than the free surface, is justified by considering the simple 2-dimensional elasticity problem of a thick-walled cylindrical shell containing a pressurized cylindrical hole, pictured below in Figure 9. For this system, elasticity theory predicts that the 2-dimensional hydrostatic stress ($\sigma_H = \sigma_{rr} + \sigma_{\theta\theta} = \sigma_{xx} + \sigma_{yy}$) at any point in the material is independent of position and,

$$\sigma_H = p\frac{R_i^2}{(R_o^2 - R_i^2)},$$

where $p$ is the pressure of the gas within the hole, $R_o$ is the outer radius of the thick-walled shell and $R_i$ is the inner radius of the shell. Since this value is constant, the volume integral of $\sigma_H$ is

$$\int_{V_{\text{shell}}} \sigma_H dV = \sigma_H * V_{\text{shell}} = p\frac{R_i^2}{(R_o^2 - R_i^2)} * \pi\left(R_o^2 - R_i^2\right) = p\pi R_i^2.$$

However, the isobaric condition used in simulation takes into account not only the stress in the material, but also the stress in the bubbles. The hydrostatic stress $\sigma_H$ for this case is

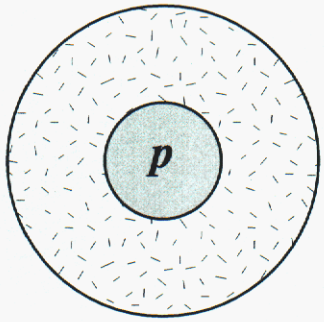


Figure 9: A thick-walled cylindrical shell containing a gas of pressure $p$

$-p$ and the volume integral is

$$\int_{V_{\text{hole}}} \sigma_H dV = -p * V_{\text{hole}} = -p\pi R_i^2.$$

Thus, the volume integral of hydrostatic stress for the entire system is

$$\int_{V_{\text{system}}} \sigma_H dV = p\pi R_i^2 - p\pi R_i^2 = 0.$$

This simple analysis shows that for only free boundaries and a pressurized hole, an elastic medium develops a hydrostatic stress that exactly balances, in a volume-averaged sense, the pressure within the hole. Thus, any discrepancy should come either from the fixed boundary, or some non-elastic aspect of the MD simulation.

The effect of a fixed bottom boundary for an elastic medium was investigated using a finite element (FE) calculation of a pressurized cylindrical hole inside a linear elastic, 2-dimensional, rectangular region. The system analyzed is pictured below in Figure 10, which shows (a) the mesh used and (b) the area integration of the normal stress $\sigma_{yy}$. The mesh in Figure 10 contains 1,609 nodes and 1,490 elements. The nodes along the bottom boundary for this region are constrained against vertical (y-direction) motion, the nodes on the side boundaries are constrained against horizontal (x-direction) motion, and the top surface is free. It was observed that for a set amount of normal surface traction on the hole, corresponding with a certain amount of pressure, it was **always** the case that material region deformed such that the area integration of normal stress $\sigma_{yy}$ roughly equaled the product of the pressure value and the area of the hole. In other words, the normal stress in the solid balanced the pressure loading of the hole in the free surface normal's direction, just as for the simple thick-walled shell already discussed. In contrast, since **both** side boundaries are constrained, only a specific amount of stretch in the horizontal direction satisfies the condition that the area integration of normal stress $\sigma_{xx}$ equals that same product of pressure and hole area. This agreement of $\int \sigma_{yy} dA = p\pi R^2$ (where $R$ is the

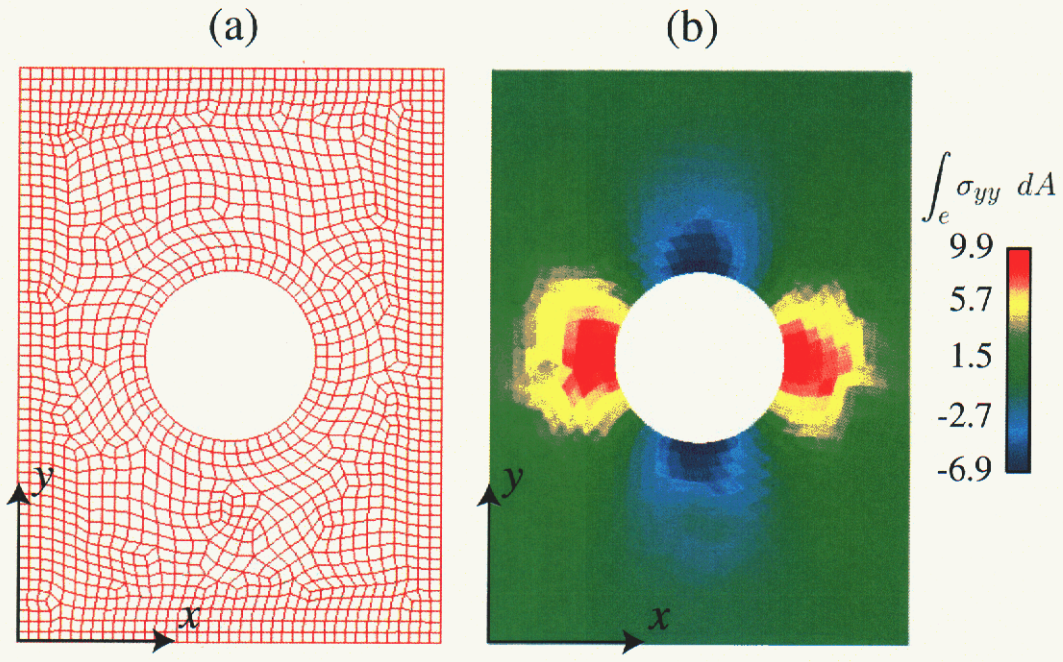


Figure 10: (a) FE mesh of a pressurized cylindrical hole in a linear elastic, 2-dimensional, rectangular region. (b) The same mesh with elements colored according the area integration of normal stress $\sigma_{yy}$.

radius of the hole) became more precise as the number of nodes and elements were increased to 8,342 and 8,043, respectively. It was also verified that for a rectangular, elastic region containing multiple pressurized cavities, pictured below in Figure 11, $\int \sigma_{yy} dA = \sum p\pi R^2$. The right hand side of this equality is just the linear summation of the product of each hole's pressure and area. Finally, the original geometry shown in Figure 10 was analyzed with an entire set of nodes fixed along the bottom of the rectangular region, not just those bordering the bottom boundary. The region was stretched horizontally (in the x-direction) so that $\int \sigma_{xx} dA = p\pi R^2$. For this situation, the area integration of $\sigma_{yy}$ **exceeded** the value of $p\pi R^2$, producing an excess tension within the system. The excess tension is an expected result as the vertical constraint of a finite-width region acts as a constraint against the Poisson contraction that would otherwise take place upon horizontal stretching of the system. However, since this stress is the opposite sign observed in the MD simulations, it does not explain the result of an excess compression.

Another possible explanation for excess compression observed is the inelastic behavior of the metal during bubble growth. Specifically, as the bubbles grow they nucleate dislocation threads in order to accommodate that growth. These dislocations relieve the tensile stress within the material that, until that point, is balancing the elastic loading of the pressure

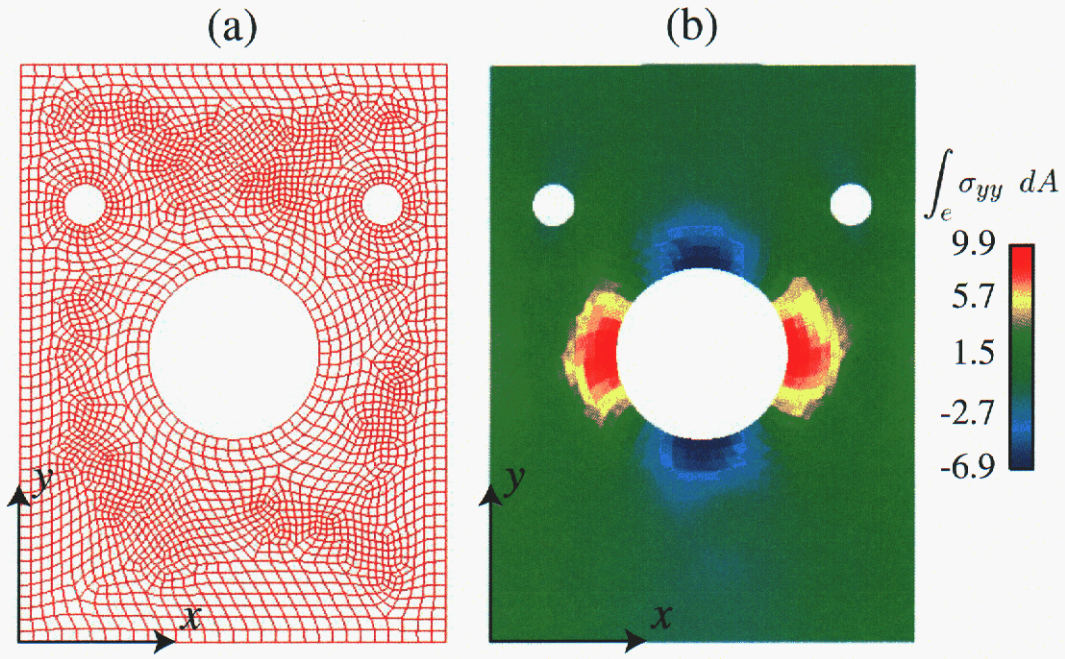


Figure 11: (a) FE mesh of a linear elastic, 2-dimensional, rectangular region with multiple pressurized holes. (b) The same mesh with elements colored according the area integration of normal stress $\sigma_{yy}$.

within the bubbles. Assuming that dislocation emission relieves most of the stress within the metal, the system stress $\sigma_{zz}$ should be approximately equal to the product of the bubble pressure and the volume fraction of He in the lattice. This possible explanation was investigated using results from an early portion of the simulation set, at a He/M ratio of 0.025 and a volume fraction of He equal to 0.013. For this volume fraction, the average bubble pressure was 90 kbar, resulting in an expected residual compression of approximately -1.17 kbar. In fact, the calculated value of $\sigma_{zz}$ for the system varied within the range of -0.09 to -1.3 kbar. At a later portion of the simulation set, He/M $\approx$ 0.07 and volume fraction $\approx$ 0.046, this was again measured. In order to eliminate thermal effects, the system's potential energy was minimized at this bubble size and zero system pressure using a conjugate gradient algorithm. This minimized system maintained a residual compression for $\sigma_{zz}$ equal to -1.22 kbar for a bubble pressure of 64.76 kbar. Once minimized, the repulsive bubble potentials are "turned-off" and the system was observed to now have a residual tension of 1.87 kbar. Since the system's average stress is a volume average of this residual tension within the metal and the pressure within the bubbles (when the bubble potentials are "turned-on"), the amount of residual compression in the system is

$$\sigma_{zz} = -64.76 * 0.046 + 1.87 = -1.1 \text{ kbar}.$$

This value is very close to the observed value of -1.22 kbar. It does appear that this explana-

tion of excess compression due to relief of stress within the metal by dislocation production is consistent with the simulation results.

One further explanation examined is the idea that the system is artificially constrained. Simulation sets from both the bulk and free surface simulations were selected and energy minimized in the manner described above. The resulting systems showed that even for a minimized configuration, the metal atoms exerted a significant, non-zero net force on each bubble. An interesting feature is that, for the bulk simulations, the vector sum of forces on all four of the bubbles is nearly zero. For example, at a He/M ratio of 0.1, the volume fraction of He for the minimized system is 0.062 and the average bubble pressure is 74.98 kbar. The sum of the forces on all bubbles in the x, y and z-directions are 0.004 eV/Å, 0.0027 eV/Å and -0.0005 eV/Å, respectively. These values are very small when compared to the individual x, y and z forces on each bubble, which ranges from -26 to 35 eV/Å. In contrast, for the free surface simulation set with bubbles of the same radius, He/M $\approx$ 0.07, volume fraction of He equals 0.045, average bubble pressure equals 48 kbar, and the sum of the forces on all bubbles in the x, y and z-directions are 0.0033 eV/Å, -0.01 eV/Å and 43.56 eV/Å, respectively. Clearly, the net force on all bubbles in the z-direction, the direction of the free surface normal, is significant and should not be ignored. As for the bulk simulations, the forces on each individual bubble are significantly non-zero and range from -25 to 34 eV/Å. The logical next step for improving the bubble growth model is to allow the bubbles to reposition themselves so that, upon energy minimization, the net force on each bubble, as well as the vector sum of the forces on all bubbles, is nearly zero. This proposed improvement will be discussed in the next section.

As stated above, for the same amount of bubble volume, the free-surface simulation predicts a higher bubble pressure than for the bulk simulations. Mechanics intuition would lead one to conclude that the presence of the free surface should make that system more compliant, and expect a lower bubble pressure. It's conceivable that the constraint of fixed bubble position is responsible for this lack of compliance. Through its impact on bubble pressure, this constraint may also be affecting the volume fraction and swelling behavior noticed earlier. Finally, the wealth of material defects present at He/M = 0.27 may indicate a critical point in the evolution of the bubble growth. More thought is required to provide the correct interpretation of this feature.

# Summary and Future Directions for Research

This research used molecular dynamics simulations to investigate the origins of material defects caused by the growth of He gas bubbles in Pd crystal lattice. Periodic, free and rigidly fixed boundary conditions were used to model bubble growth near a free surface in a sample of macroscopic thickness, and were compared with previously-determined results for bubble growth within a bulk lattice [1]. Simulation results for both systems conflict with pre-conceived theories of dislocation loop punching. They show bubble pressure monotonically decreasing with He concentration and the formation of threading dislocations as opposed to prismatic loops. Since these characteristics are seen in both free surface and bulk simulations, the implementation of the fixed boundary condition does not alter this finding. By their nature, the simulations more accurately predict the features of atomic-scale defects than conventional continuum theories. They also allow the visualization of defects and processes that are intractable at the experimental scale. The types of defects created were similar for both systems, although the presence of a free surface noticeably affects their distribution.

Several features observed for the free surface simulations were not expected and are counter-intuitive. For a given volume of He gas, the free surface system reached a higher average bubble pressure than did the bulk system. This higher pressure is not consistent with the observation that the free surface system has increased swelling over the bulk system for a given He/M ratio. These characteristics may be connected to a build-up of compressive normal stress in the free surface normal's direction. Several possible causes for this build-up were noted and investigated, including the rigid boundary condition for the bottom atomic layer, relaxation of stress within the metal due to the formation of dislocations and other material defects, and the artificial constraint imposed by holding the bubble centers fixed relative to the simulation geometry.

Future work for this project will involve the isolation and elimination of the origin of the excess compression that was observed in the free surface simulations. A series of simulations will be performed to study He bubble growth within a Pd thin-film, *i.e.* free boundary conditions on both the top and bottom surfaces. These simulations will help characterize the influence of the rigid boundary condition present in the simulations discussed in this report. It was noted previously that by constraining the position of the bubble centers, the metal atoms exert a significantly non-zero net force on each bubble for both bulk and free surface simulations. The bubble growth algorithm will be modified to include extra degrees of freedom for each bubble. Hence, each bubble will have its own "equation of motion", and will move according to the direction and magnitude of these forces. The mass attributed to each bubble will be estimated from the number of He atoms each bubble contains (calculated according to the same equation of state used for this work, detailed in Appendix B of [1]) times the atomic mass of Pd atoms, rather than the mass of He atoms. Preliminary simulations done prior to the completion of this report indicate that the heavier mass is necessary to ensure physically realistic motion of the bubbles at small bubble volumes. Also, it has been experimentally observed that bubbles move only by preferential growth in certain directions, rather than by "plowing" past surrounding metal atoms [19]. Thus, a maximum

displacement per time-step will be enforced to ensure that each bubble does not move more than the amount of increase of its radius. Once these modifications have been implemented and tested, future simulations will correct the unanticipated behavior mentioned above and provide more insight into the physical mechanisms that are active to create material defects during He bubble growth, and how these defects interact and lead to the accelerated release of He gas.

# References

[1] S.M. Foiles and J.J. Hoyt. Computer Simulation of Bubble Growth in Metals Due to He. Technical Report SAND2001-0661, Sandia National Laboratories, 2001.

[2] R. Causey. Interaction of helium with dislocations in metals: Mini review. 2001.

[3] S. Thiébaut, B. Décamps, J.M. Pénisson, B. Limacher, and A. Percheron Guégan. TEM study of the aging of palladium-based alloys during tritium storage. *Journal of Nuclear Materials*, 277:217–225, 2000.

[4] A. Ryazanov, H. Matsui, and A.V. Kazaryan. Physical mechanisms of helium release during deformation of vanadium alloys doped with helium atoms. *Journal of Nuclear Materials*, 271&272:356–359, 1999.

[5] G.C. Abell, L.K. Matson, R.H. Steinmeyer, R.C. Bowman Jr., and B.M. Oliver. Helium release from aged palladium tritide. *Physical Review B*, 41(2):1220–1223, 1990.

[6] J.A. Emig, R.G. Garza, L.D. Christensen, P.R. Coronado, and P.C. Souers. Helium release from 19-year-old palladium tritide. *Journal of Nuclear Materials*, 187:209–214, 1992.

[7] D.C. Chrzan and W.G. Wolfer. Helium bubble growth by the dislocation pipe diffusion mechanism. Technical Report SAND91-8671, Sandia National Laboratories, 1991.

[8] W.G. Wolfer. The pressure for dislocation loop punching by a single bubble. *Philosophical Magazine A*, 58(2):285–297, 1988.

[9] W.G. Wolfer. Dislocation loop punching in bubble arrays. *Philosophical Magazine A*, 59(1):87–103, 1989.

[10] W.G. Wolfer and W.J. Drugan. Elastic interaction energy between a prismatic dislocation loop and a spherical cavity. *Philosophical Magazine A*, 57(6):923–927, 1988.

[11] J.B. Adams, W.G. Wolfer, S.M. Foiles, C.M. Rohlfing, and C.D. Van Siclen. Theoretical studies of helium in metals. In S.E. Donnelly and J.H. Evans, editors, *Fundamental Aspects of Inert Gases in Solids*, Proceedings of a NATO Advanced Research Workshop, pages 3–16. NATO, 1991.

[12] F.F. Abraham, D. Brodbeck, W.E. Rudge, J.Q. Broughton, D. Schneider, B. Land, D. Lifka, J. Gerner, M. Rosenkrantz, J. Skovira, and H. Gao. *Ab initio* dynamics of rapid fracture. *Modelling and Simulation in Materials Science and Engineering*, 6:639–670, 1998.

[13] F.F. Abraham and H. Gao. Anomalous ductile-brittle fracture behavior in fcc crystals. *Philosophical Magazine Letters*, 78:307–312, 1998.

[14] M.P. Allen and D.J. Tildesley. *Computer Simulation of Liquids.* Clarendon Press, Oxford, 1987.

[15] M.S. Daw and M.I. Baskes. Embedded-atom-method: Derivation and application to impurities, surfaces, and other defects in metals. *Physical Review B*, 29(12):6443–6453, 1984.

[16] S.M. Foiles, M.I. Baskes, and M.S. Daw. Embedded-atom-method functions for the fcc metals Cu, Ag, uppercaseAu, Ni, Pd, Pt, and their alloys. *Physical Review B*, 33(12):7983–7991, 1986.

[17] S. Plimpton. Fast parallel algorithms for short-range molecular dynamics. *Journal of Computational Physics*, 117:1–19, 1995.

[18] C.L. Kelchner, S.J. Plimpton, and J.C. Hamilton. Dislocation nucleation and defect structure during surface indentation. *Physical Review B*, 58:11085–11088, 1998.

[19] D.F. Cowgill. private communication, 2002.

[20] W.G. Wolfer. The elastic properties of aged palladium tritides. Technical Report SAND90-8253, Sandia National Laboratories, 1990.

[21] S.E. Guthrie. Helium effects on palladium hydride equilibrium properties. Technical Report SAND90-8233, Sandia National Laboratories, 1990.

[22] S.H. Goods and S.E. Guthrie. Mechanical properties of palladium and palladium hydride. Technical Report SAND91-8702, Sandia National Laboratories, 1991.

[23] G.C. Abell and A. Attalla. NMR evidence for solid-fluid transition near 250 K of $^3$He bubbles in palladium tritide. *Physical Review Letters*, 59(9):995–997, 1987.

# Acronyms and Symbols

| | |
|---|---|
| EAM | Embedded Atom Method |
| FCC | face centered cubic |
| FE | finite element |
| He | helium |
| LP | loop punching |
| M | metal |
| MD | molecular dynamics |
| MPI | Message Passing Interface |
| Pd | palladium |
| PdH | palladium hydride |
| PdT | palladium tritide |

This page intentionally left blank.

# DISTRIBUTION:

| | | |
|---|---|---|
| 1 | MS 0316 | J.B. Aidun, 9235 |
| 1 | | S.J. Plimpton, 9212 |
| 1 | MS 0516 | R.G. Spulak, 2564 |
| 1 | MS 0521 | F.M. Bacon, 2502 |
| 1 | MS 0824 | A.C. Ratzel, 9110 |
| 1 | MS 0841 | T.C. Bickel, 9100 |
| 1 | MS 0847 | H.S. Morgan, 9120 |
| 1 | MS 0871 | L.C. Beavis, 14405 |
| 1 | MS 0885 | G.S. Heffelfinger, 1802 |
| 1 | MS 0886 | P.G. Kotula, 1822 |
| 1 | MS 1411 | H.E. Fang, 1834 |
| 1 | | S.M. Foiles, 1834 |
| 1 | | J.J. Hoyt, 1834 |
| 1 | MS 1427 | J.M. Phillips, 1100 |
| 1 | MS 9001 | M.E. John, 8000<br>Attn:<br>J. Vitko, 8100, MS 9004<br>D.R. Henson, 8200, MS 9007<br>W.J. McLean, 8300, MS 9054<br>P.N. Smith, 8500, MS 9002<br>K.E. Washington, 8900, MS 9003 |
| 1 | MS 9052 | S.F. Rice, 8361 |
| 1 | MS 9108 | R.D. Monson, 8243 |
| 1 | | C.A. Lajeunesse, 8243 |
| 1 | | C.W. Pretzel, 8243 |
| 1 | | S.L. Robinson, 8243 |
| 1 | | G.C. Story, 8243 |
| 1 | MS 9161 | E.P. Chen, 8726 |
| 1 | | P.A. Klein, 8726 |

| | | |
|---|---|---|
| 1 | | D.A. Zeigler, 8726 |
| 15 | | J.A. Zimmerman, 8726 |
| 1 | MS 9202 | R.M. Zurn, 8205 |
| 1 | MS 9402 | C.H. Cadden, 8724 |
| 1 | | R. Causey, 8724 |
| 1 | | D.F. Cowgill, 8724 |
| 1 | | K.L. Hertz, 8724 |
| 1 | | B.P. Somerday, 8724 |
| 1 | MS 9403 | J.C.F. Wang, 8723 |
| 1 | | A.J. Antolak, 8723 |
| 1 | | E.H. Majzoub, 8723 |
| 1 | | D.H. Morse, 8723 |
| 1 | MS 9405 | R.H. Stulen, 8700<br>Attn:<br>G.D. Kubiak, 8705, MS 9409<br>R.Q. Hwang, 8721, MS 9161<br>W.R. Even Jr., 8722, MS 9403<br>J.R. Garcia, 8725, MS 9042<br>C.C. Henderson, 8729, MS 9401<br>J.E.M. Goldsmith, 8730, MS 9409<br>W.C. Replogle, 8731, MS 9409 |
| 1 | MS 9405 | K.L. Wilson, 8703 |
| 1 | LANL | B.A. Meyer,ESA-GTS, C934 |
| 1 | | K.G. Honnell, ESA-GTS, C934 |
| 1 | LLNL | W.G. Wolfer,L353 |
| 1 | | C.R. Krenn, L353 |
| 1 | | K.A. Winer, L170 |
| 1 | | S. Sack, L170 |
| 3 | MS 9018 | Central Technical Files, 8945-1 |
| 1 | MS 0899 | Technical Library, 9616 |
| 1 | MS 9021 | Classification Office, 8511/<br>Technical Library, MS 0899, 9616 |
| 1 | | DOE/OSTI via URL |